INTERNATIONAL JOURNAL OF SCIENCE TECHNOLOGY EDUCATION ENTERPRENEURSHIP AND MANAGEMENT (IJ-STEEM)
ISSN: 3093-0898 Journal homepage: https://atbuijsteem.com.ng/journal

270 V DC POWER SYSTEMS FOR ELECTRIC VEHICLE DRIVE APPLICATIONS: MODELING AND SIMULATION

By
Mutiat Shittu Yisa*
Federal University of Technology, Minna. Niger State.
*Corresponding author: Email: yisashittu@futminna.edu.ng (Tel: +234 08032271965)

Abstract

The rapid electrification of road transportation demands efficient and reliable power conversion solutions for high-performance electric vehicle (EV) drive systems. This paper presents the modelling and simulation of an Insulated Gate Bipolar Transistor (IGBT)-based Active Front-End (AFE) rectifier for 270 V DC bus applications in EVs. The proposed system regulates the DC-link voltage while maintaining near-sinusoidal input currents and unity power factor. The AFE rectifier is modelled in the synchronous dqreference frame and controlled using cascaded voltage and current loops implemented in MATLAB/Simulink. Proportional–Integral (PI) controllers are designed via closed-loop transfer function analysis to achieve fast transient response and robustness against line and load variations. Simulation studies under steady-state, dynamic, and transient conditions demonstrate effective harmonic suppression, stable DC-link voltage, and improved power quality. The results indicate that the proposed AFE rectifier control scheme is a practical solution for 270 V DC bus regulation, supporting the integration of onboard chargers, battery packs, and traction motor drives in electric vehicles.

Keywords: Active Front-End (AFE), DC-link voltage regulation, Electric vehicles, PI control, Power quality, Traction drives.

Introduction

The rapid shift toward sustainable transportation is driving increased demand for highly efficient and reliable electrical power systems in electric vehicles (EVs) and hybrid electric vehicles (HEVs). At the heart of these systems is the power conversion stage, which governs energy exchange among the grid, the battery storage system, and the motor drive [1]. Selecting an appropriate DC-link voltage is essential for maintaining power quality, optimizing efficiency, and ensuring overall system stability across diverse operating conditions.

Early generations of EV power electronic systems primarily employed low-voltage (12/48V) architectures and unidirectional converters dedicated to auxiliary loads, whereas the increasing requirements for traction power and onboard charging have shifted

INTERNATIONAL JOURNAL OF SCIENCE TECHNOLOGY EDUCATION ENTERPRENEURSHIP AND MANAGEMENT
(IJ-STEEM)
ISSN: 3093-0898 Journal homepage: https://atbuijsteem.com.ng/journal

research focus toward higher DC-link voltages and bidirectional converter topologies [2]. Within this technological evolution, voltage-source Active Front-End (AFE) rectifiers have become a key interface for regulated DC buses, as they provide near-unity power factor, low input harmonic distortion, and regenerative capability, all of which closely match the demands of EV charging and drive-cycle operation [3,4]. A regulated 270 V DC bus has consequently emerged as a promising solution, particularly for medium-voltage EV platforms, heavy-duty vehicles, and specialized applications such as electric buses and construction machinery [5].

A 270 V DC architecture enables reduced conductor cross-sections due to lower current levels, enhances inverter efficiency by mitigating switching stress, and offers a practical compromise between safety constraints and performance requirements [6,7]. Furthermore, its alignment with standard semiconductor voltage ratings and common battery pack configurations strengthens its suitability as an intermediate DC-link level in EV powertrains. Despite these benefits, realizing robust voltage regulation and preserving high power quality at this voltage level remains challenging, especially under dynamic operating conditions such as acceleration, regenerative braking, and DC fast charging [8].

Modelling approaches for AFE rectifiers range from detailed switching models to averaged synchronous dq-frame representations. Switching models describe device-level behavior and PWM-induced ripple with high fidelity but are often computationally prohibitive for system-level studies and systematic controller synthesis [9,10]. In contrast, averaged dq-frame models support control-oriented analysis by providing a clear separation between active-power (d-axis) and reactive-power (q-axis) control channels, thereby enabling tractable assessment of bandwidth, stability margins, and disturbance rejection for EV operating conditions, including acceleration and braking transients as well as grid- and charger-induced perturbations [11,12]

Regarding control strategies, cascaded control structures with an outer DC-link voltage loop and an inner current loop remain the de facto standard because of their robustness and transparency in design [13],[14]. The inner current loop typically employs PI regulators with cross-coupling compensation terms ($\pm\omega L$) to decouple the d–q dynamics, while the outer loop regulates the DC bus voltage by generating the active-current reference i_d^*. Advanced implementations further incorporate grid-voltage feedforward, disturbance observers, and anti-windup schemes to improve performance under large transients [15,16,17]. Phase-locked loop (PLL) synchronization is also essential; grid-connected EV chargers and hybrid/EV generators commonly use robust PLL schemes, such as synchronous-reference-frame PLL (SRF-PLL) variants, to maintain accurate phase alignment and resilience against harmonics and grid voltage sags [18].

INTERNATIONAL JOURNAL OF SCIENCE TECHNOLOGY EDUCATION ENTERPRENEURSHIP AND MANAGEMENT
(IJ-STEEM)
ISSN: 3093-0898 Journal homepage: https://atbuijsteem.com.ng/journal

Alternative control schemes for AFE rectifiers include resonant controllers, H_∞/μ-synthesis, and model predictive control (MPC), which have been introduced to enhance harmonic suppression, robustness against parameter variations, and transient response in demanding operating conditions [19,20,21]. Although these advanced methods can surpass conventional PI control within certain operating ranges, they typically involve higher computational complexity, more intricate tuning procedures, and reduced transparency, all of which complicate certification and real-time deployment in automotive Electronic Control Units (ECUs). As a result, carefully tuned PI controllers with dq-axis decoupling remains the dominant choice in production-oriented systems, particularly when supported by accurate plant identification and clear bandwidth separation between the voltage and current control loops [22].

In terms of modulation strategies, sinusoidal PWM (SPWM) is widely adopted because of its simplicity and well-characterized harmonic spectrum, whereas space-vector PWM (SVPWM) achieves superior DC bus utilization and slightly reduced switching losses, benefits that become more pronounced at higher modulation indices and over wider operating ranges [23]. For 270 V EV DC buses, both SPWM and SVPWM are technically feasible, and the final selection is often driven by controller sampling limits and electromagnetic interference (EMI) constraints. EMI/EMC compliance continues to be a critical design driver in automotive power electronics, where spread-spectrum PWM techniques and carefully optimized input/output filter designs are used to satisfy CISPR and ISO regulatory standards without incurring excessive cost, volume, or weight [24].

From this review, many high-fidelity AFE rectifier models are unsuitable for EV drive-cycle analysis and controller tuning because their computational burden is excessive, whereas several reduced-order or small-signal models neglect important large-signal effects, including non-minimum phase behaviour relevant during step torque changes and regenerative braking. At the same time, advanced control schemes can surpass PI performance only in specific operating niches, often at the cost of increased implementation complexity and reduced transparency, which limits their practicality in automotive applications.

These observations motivate an AFE–CRU framework that: (i) employs a dq-averaged model with explicit decoupling and feedforward, enabling robust cascaded PI control; (ii) targets a 270 V DC-link representative of medium-voltage EV platforms; and (iii) is validated under realistic load transients corresponding to acceleration, grade variation, and regenerative events [25]. Such a framework offers a balanced compromise between model fidelity, interpretability, and computational tractability, making it well suited for EV-oriented design and control workflows. The remainder of this paper is structured as follows: Section II introduces the overall system architecture and control strategy, Section III details the AFE rectifier modelling in the synchronous dqreference

INTERNATIONAL JOURNAL OF SCIENCE TECHNOLOGY EDUCATION ENTERPRENEURSHIP AND MANAGEMENT (IJ-STEEM)
ISSN: 3093-0898 Journal homepage: https://atbuijsteem.com.ng/journal

frame, Section IV presents simulation results under diverse loading scenarios, and Section V summarizes key findings and outlines prospective research directions.

System Architecture and Control Strategy

Overview of the 270 V DC Power System

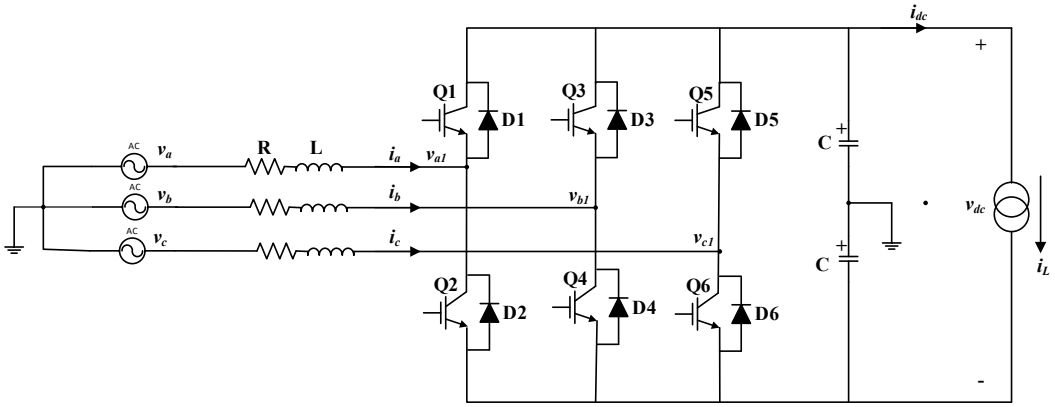

Figure 2. Three-phase two-Level AFE converter

The proposed system regulates a 270 V DC bus for electric vehicle (EV) drive applications. At its core is an AFE rectifier, enabling bidirectional power flow between the AC source (representing either the grid during charging or an onboard generator in hybrid configurations) and the DC bus. The AFE ensures tight voltage regulation while shaping AC input currents to meet harmonic distortion and power factor requirements [26].

The 270 V DC bus functions as the central interface linking the main subsystems: the traction motor drive through a voltage-source inverter, the battery or energy storage system through a bidirectional DC/DC converter, and auxiliary loads such as HVAC, lighting, and control electronics through appropriate step-down converters. This work considers a single-source configuration in which a Permanent Magnet Synchronous Generator (PMSG) supplies power to the DC bus via the AFE rectifier, as illustrated conceptually in Figure 1, with future extensions planned for multi-source topologies involving two or more generators. Such an architecture facilitates centralized energy management and supports efficient allocation of the available power between propulsion and non-propulsion loads, thereby improving overall system effectiveness in EV applications.

Active Front-End Rectifier (AFE CRU)

The AFE rectifier is implemented as a three-phase Voltage Source Converter (VSC) using Insulated Gate Bipolar Transistors (IGBTs), as depicted in Figure 2. Its primary functions are to regulate the DC-link voltage at 270 V across all loading conditions, achieve near-unity power factor at the AC input by controlling the input current phase angle, attenuate low-order harmonics to satisfy automotive power quality standards (e.g.,

INTERNATIONAL JOURNAL OF SCIENCE TECHNOLOGY EDUCATION ENTERPRENEURSHIP AND MANAGEMENT
(IJ-STEEM)
ISSN: 3093-0898 Journal homepage: https://atbuijsteem.com.ng/journal
IJ-STEEM

ISO 7637, IEC 61000), and enable regenerative braking energy to be returned to the grid or stored in the battery pack [27].

Rectifier operation is governed by Sinusoidal Pulse Width Modulation (SPWM) of the IGBTs, while the anti-parallel diodes provide a natural freewheeling path for the input current during switching transitions, thereby supporting bidirectional power flow [28]. Consequently, the AFE–CRU performs both rectification and controlled regeneration to the AC mains, which is essential in automotive applications that require efficient energy recovery during regenerative braking. The converter is controlled in the synchronous dq-reference frame, where the control variables are decomposed into active (d-axis) and reactive (q-axis) components, simplifying the design and tuning of the current and voltage controllers [28].

The DC-link capacitor is crucial for maintaining voltage stability on the DC side by filtering the ripple induced by converter switching [29],[30] and it's sizing strongly influences the dynamic response, voltage ripple level, and harmonic content on the DC bus , . This fundamental topology forms the basis for subsequent analysis of converter dynamics, control strategy development, and performance assessment under diverse loading and operating conditions.

Control Strategy

The 270 V DC bus is controlled using a hierarchical cascaded control structure comprising an outer voltage loop and an inner current loop, as illustrated in Figure 1. The outer loop regulates the DC-link voltage and generates the d-axis current reference i_d^*, while the inner loop regulates the d- and q-axis currents, $i_d$and i_q, using PI controllers with appropriate feedforward decoupling terms [31].

To ensure effective decoupling of the dq-axis dynamics, feedforward compensation is incorporated so that the cross-coupling terms are counteracted within the inner current loop. The current loop is designed with a higher bandwidth than the voltage loop to achieve fast current tracking and strong disturbance rejection, whereas the voltage loop operates more slowly to shape the active power flow via the d-axis current reference.

Modelling of the AFE Rectifier in the Synchronous dq-Reference Frame

The AFE rectifier is modelled in the synchronous rotating reference frame (dq-frame) so that AC quantities appear as DC variables under steady-state conditions, which greatly simplifies their control in EV applications. This modelling approach facilitates independent regulation of active and reactive power, since the d- and q-axis components can be handled by decoupled control loops.

1) ***Reference frame transformation***

To enable effective control of the AFE-CRU, the original three-phase system equations are reformulated in a rotating reference frame aligned with the grid voltage. Direct control of the three-phase input voltages $v_{abc}$is difficult because they are sinusoidal and time-varying, so they are first mapped into the stationary $\alpha\beta$frame via the Clarke transformation, where the quantities become easier to analyze and form the basis for subsequent conversion into the synchronous dqframe [32].

INTERNATIONAL JOURNAL OF SCIENCE TECHNOLOGY EDUCATION ENTERPRENEURSHIP AND MANAGEMENT
(IJ-STEEM)
ISSN: 3093-0898 Journal homepage: https://atbuijsteem.com.ng/journal

$$\begin{bmatrix} v_\alpha \\ v_\beta \end{bmatrix} = \frac{2}{3}\begin{bmatrix} 1 & -\frac{1}{2} & -\frac{1}{2} \\ 0 & \frac{\sqrt{3}}{2} & -\frac{\sqrt{3}}{2} \end{bmatrix}\begin{bmatrix} v_a \\ v_b \\ v_c \end{bmatrix} \quad (1)$$

Although the Clarke transformation removes redundancy by mapping three-phase quantities into the stationary $\alpha\beta$ frame, the resulting signals remain sinusoidal and time-varying. Subsequently, the Park transformation is applied to rotate the $\alpha\beta$ frame into the synchronous dq frame, aligned with the grid voltage vector angle θ, so that under steady-state conditions the transformed variables become constant and are suitable for DC-like control implementation [32].

$$\begin{bmatrix} v_d \\ v_q \end{bmatrix} = \frac{2}{3}\begin{bmatrix} \cos\theta & \sin\theta \\ -\sin\theta & \cos\theta \end{bmatrix}\begin{bmatrix} v_\alpha \\ v_\beta \end{bmatrix} \quad (2)$$

In this formulation, θ denotes the instantaneous grid voltage angle, which is estimated using a phase-locked loop (PLL). The d-axis is aligned with the grid voltage vector so that the d-axis current directly represents active power transfer, while the q-axis current is associated with reactive power exchange [31]. By independently regulating the d- and q-axis currents, the AFE–CRU can enforce near-unity power factor, reduce input current harmonics, and tightly control the DC-link voltage to meet EV power quality and performance requirements.

2) Plant model in the dq frame

Neglecting measurement delays and PWM switching effects, the dynamics of the rectifier-side AC currents in the synchronous dq reference frame can be expressed [33]:

$$\left.\begin{aligned} v_d &= Ri_d + L\frac{di_d}{dt} - \omega_e L i_q + v_{d1}, \\ v_q &= Ri_q + L\frac{di_q}{dt} + \omega_e L i_d + v_{q1}, \end{aligned}\right\} \quad (3)$$

where R and L are the AC-side resistance and inductance, ω_e is as a set of coupled first-order differential equations that relate the d- and q-axis currents to the corresponding converter voltage commands, grid voltages, and filter parameters. This representation captures the dominant low-frequency behavior of the AFE rectifier while remaining simple enough for control design and stability analysis in EV applications.

In these expressions, R and L denote the AC-side resistance and inductance, ω_e is the electrical angular frequency, i_d and i_q are the dq-axis currents, and v_{d1}, v_{q1} are the dq-axis control voltages synthesized by the AFE converter. The dq-frame current dynamics are

INTERNATIONAL JOURNAL OF SCIENCE TECHNOLOGY EDUCATION ENTERPRENEURSHIP AND MANAGEMENT
(IJ-STEEM)
ISSN: 3093-0898 Journal homepage: https://atbuijsteem.com.ng/journal

intrinsically coupled through the cross terms proportional to ωL, which link the d- and q-axis states and complicate independent current regulation.

To enable decoupled control of $i_d$and i_q, feedforward compensation terms are added in the current controllers, as expressed in (4) [34], so that the cross-coupling components are effectively canceled and each axis approximates a first-order system. In addition, grid-voltage feedforward is incorporated to enhance disturbance rejection, particularly during load steps and grid-voltage perturbations, thereby improving dynamic performance of the AFE–CRU.

To realize this decoupling, the commanded control voltages are shaped as:
To decouple the channels, we command

$$\left.\begin{aligned} v_{d1}^{*} &= v_d - \underbrace{(-\omega_e L i_q)}_{cross-coupling} + v_d^{'}, \\ v_{q1}^{*} &= v_q - \underbrace{(+\omega_e L i_d)}_{cross-coupling} + v_q^{'}, \end{aligned}\right\} \qquad (4)$$

where $v_{d,\mathrm{ctrl}}^{*}$and $v_{q,\mathrm{ctrl}}^{*}$are the outputs of the d- and q-axis PI regulators, and $v_{d,\mathrm{ff}}, v_{q,\mathrm{ff}}$represent the grid-voltage feedforward components. This structure yields approximately decoupled current loops, which simplifies controller tuning and supports robust performance over the EV operating envelope.

so that the inner controllers act on the "reduced" plants

$$\left.\begin{aligned} G_{id}(s) &= \frac{I_d(s)}{V_d^{'}(s)} = \frac{1}{Ls+R}, \\ G_{iq}(s) &= \frac{I_q(s)}{V_q^{'}(s)} = \frac{1}{Ls+R}. \end{aligned}\right\} \qquad (5)$$

3) Inner current controllers

The inner control loop directly regulates the converter currents in the synchronous dqreference frame, specifically the d-axis current $i_d$and q-axis current i_q, where $i_d$is associated with active power and $i_q$with reactive power. Two independents Proportional–Integral (PI) controllers are employed to track the $i_d$and $i_q$references, enabling accurate current regulation and fast dynamic response, with the controller gains obtained from the corresponding system transfer functions.

$$\left.\begin{aligned} C_{id}(s) &= k_{pd} + \frac{k_{id}}{s}, \\ C_{iq}(s) &= k_{pq} + \frac{k_{iq}}{s}. \end{aligned}\right\} \qquad (6)$$

With unity feedforward of the grid voltages $v_d, v_q$and appropriate compensation of the cross-coupling terms, the closed-loop current dynamics in each axis reduce to an approximately second-order system. Under these conditions, the d- and q-axis current

INTERNATIONAL JOURNAL OF SCIENCE TECHNOLOGY EDUCATION ENTERPRENEURSHIP AND MANAGEMENT
(IJ-STEEM)
ISSN: 3093-0898 Journal homepage: https://atbuijsteem.com.ng/journal

responses can be shaped via PI tuning to achieve desired natural frequency and damping, providing predictable transient behavior and simplifying bandwidth coordination with the outer voltage loop.

$$\left.\begin{aligned}\frac{I_d(s)}{I_d^*(s)} &\approx \frac{k_{pd}s + k_{id}}{Ls^2 + (R + k_{pd})s + k_{id}},\\ \frac{I_q(s)}{I_q^*(s)} &\approx \frac{k_{pq}s + k_{iq}}{Ls^2 + (R + k_{pq})s + k_{iq}}.\end{aligned}\right\} \quad (7)$$

Matching to the standard form

$$\frac{\omega_{ni}^2}{s^2 + 2\zeta_i\omega_{ni}s + \omega_{ni}^2}, \quad (8)$$

yields the well-known tuning relations

$$\left.\begin{aligned}k_p(\cdot) &= 2\zeta_i\omega_{ni}L - R,\\ k_i(\cdot) &= \omega_{ni}^2 L,\end{aligned}\right\} \quad (9)$$

where ω_{ni} is the current-loop natural frequency (rad/s) and ζ_i the damping ratio. In practice, ω_{ni} is selected such that

$$\omega_{ni} \leq 0.1 - 0.2\omega_s, \quad (10)$$

with $\omega_s = 2\pi f_{sw}$ the switching angular frequency, to avoid excessive modulation delay interaction [35]. In this paper, the current loop is designed with a bandwidth of 200 Hz, while the outer voltage loop has a slower bandwidth of 10 Hz to ensure hierarchical stability. Controller gains k_p and k_i are tuned to achieve a damping ratio of 0.707. The calculated PI controller gain parameters are obtained as $k_p(.) = 1.677$ and $k_i(.) = 1579.137$. Since unity power factor is desired, we set the reference $i_q^* = 0$. Reactive power control, if needed, is achieved by commanding $i_q^* \neq 0$.

4) Outer DC-link voltage controller

The primary role of the outer control loop is to regulate the DC-link voltage around its reference value, thereby guaranteeing a stable and reliable supply to the downstream loads or connected DC bus. Because the DC-link dynamics are inherently slower than the AC-side current dynamics, this voltage loop is intentionally designed with a lower bandwidth than the inner current loop, and its output is the reference for the d-axis current i_d^*, which governs active power flow.

The DC-link capacitor dynamics can be described by an energy balance relation that links the capacitor voltage to the net power exchange between the AFE rectifier and the DC-side loads, forming the basis for deriving the voltage-loop transfer function and tuning the outer PI controller.

INTERNATIONAL JOURNAL OF SCIENCE TECHNOLOGY EDUCATION ENTERPRENEURSHIP AND MANAGEMENT
(IJ-STEEM)
ISSN: 3093-0898 Journal homepage: https://atbuijsteem.com.ng/journal

$$C\frac{dv_{dc}}{dt} = i_{dc} - i_L, \tag{11}$$

where C is the DC bus capacitance, v_{dc} is the bus voltage, i_{dc} is the current drawn by the downstream loads such as the inverter, battery, or auxiliary converters, and i_L the net DC load current. In order to simplify the analysis, i_L is assumed to be zero. Using the standard

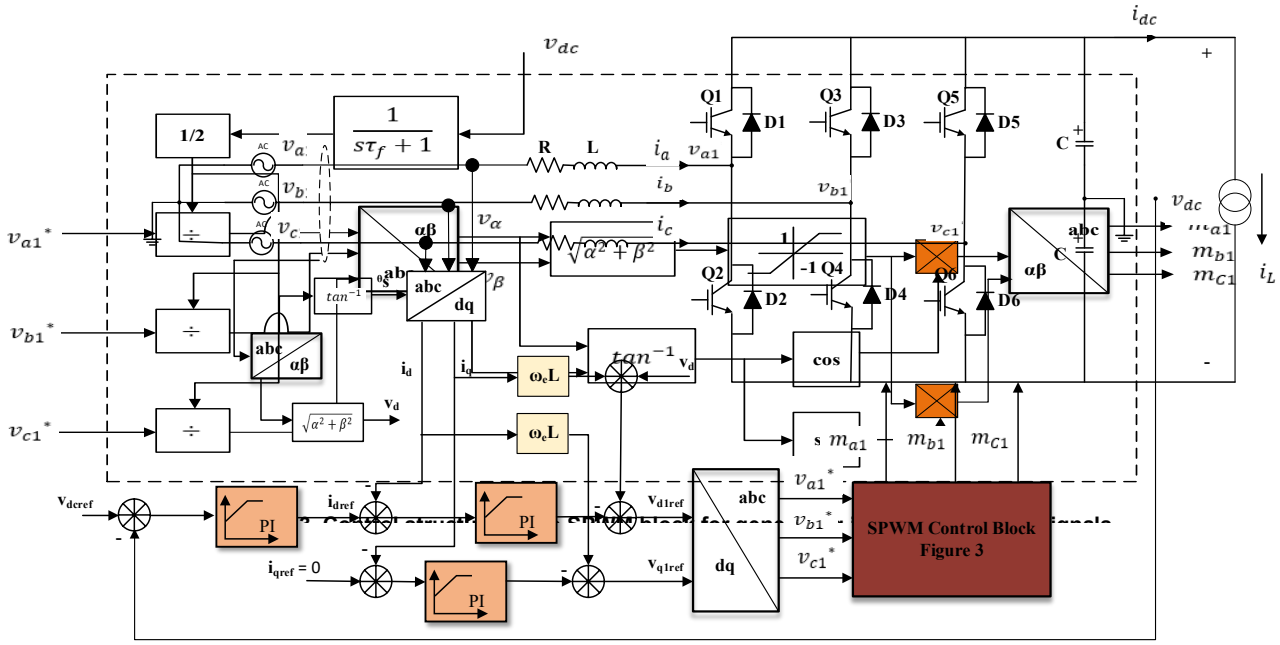

power balance approximation

$$P_{dc} = v_{dc} i_{dc} \approx \frac{3}{2}(v_d i_d + v_q i_q), \tag{12}$$

and with voltage-oriented alignment ($v_q = 0$) and $i_q \to 0$, we get

$$C\frac{dv_{dc}}{dt} \approx \frac{3}{2}\left(\frac{v_d}{v_{dc}}\right) i_d. \tag{13}$$

Linearizing around (v_{dc},i_d) and treating 3/2(v_d/v_{dc}) as a constant gain K_m, the voltage-to-current small-signal plant becomes

$$G_v(s) = \frac{V_{dc}(s)}{I_d(s)} \approx \frac{Km}{Cs}. \tag{14}$$

The outer PI controller

$$C_v(s) = k_{pv} + \frac{k_{iv}}{s} \tag{15}$$

closes the loop to yield a second-order behaviour:

INTERNATIONAL JOURNAL OF SCIENCE TECHNOLOGY EDUCATION ENTERPRENEURSHIP AND MANAGEMENT
(IJ-STEEM)
ISSN: 3093-0898 Journal homepage: https://atbuijsteem.com.ng/journal

$$\frac{V_{dc}(s)}{V_{dc}^{*}(s)} \approx \frac{K_m(k_{pv}s + k_{iv})}{s^2 + K_m k_{pv} s + K_m k_{iv}}. \quad (16)$$

Matching to ω_{nv}, ζ_v gives

$$\left.\begin{aligned} k_{pv} &= \frac{2\zeta_v \omega_{nv}}{K_m}, \\ k_{iv} &= \frac{\omega_{nv}^2}{K_m}. \end{aligned}\right\} \quad (17)$$

For the voltage controller, the natural frequency and damping ratio are set to 10 Hz ($\omega_{n,v} = 2\pi \times 10$ rad/s)and 0.707, respectively, ensuring a well-damped response of the DC-link voltage. In line with common design practice, the outer voltage-loop bandwidth is selected to be roughly one-tenth of the inner current-loop bandwidth to guarantee stable, well-coordinated cascaded control while remaining within the limits imposed by the converter switching frequency.

Table 1: System Parameters

Symbol	Quantity/Description	Value
V_s	System supply voltage	115 V rms
R	AC side resistance	0.1 Ω
L	AC side inductor	1 mH
C	DC-link capacitance	2.4 mF
R_L	DC side load resistance	40 Ω
F	System frequency	400 Hz
f_{sw}	Switching frequency	10 kHz
v_{dc}^{*}	Reference DC-link voltage	270 V DC
k_{pv}	Voltage loop proportional gain	0.316
k_{iv}	Voltage loop integral gain	14.037
$k_{pd,q}$	Current loop proportional gain	1.677
$k_{id,q}$	Current loop integral gain	1579.137

Using these specifications, the PI gains for the DC-link voltage controller are obtained as $k_{p,v} = 0.316$and $k_{i,v} = 14.037$, providing adequate dynamic performance without exciting high-frequency dynamics. This dq-frame modeling and control design framework underpins advanced vector-control implementations, enabling precise regulation of the 270 V DC bus while satisfying automotive power quality and electromagnetic compatibility requirements, which makes the approach well suited for EV applications where both power quality and transient response are critical [26].

INTERNATIONAL JOURNAL OF SCIENCE TECHNOLOGY EDUCATION ENTERPRENEURSHIP AND MANAGEMENT (IJ-STEEM)
ISSN: 3093-0898 Journal homepage: https://atbuijsteem.com.ng/journal

Simulation Results and Discussion

Time-domain simulations were carried out in MATLAB/Simulink to validate the performance of the proposed 270 V DC power system. The simulation model incorporates the Active Front-End (AFE) rectifier and the 270 V DC bus, with the AFE described in the synchronous dq-reference frame and controlled via decoupled voltage and current loops tuned to ensure stability and adequate dynamic response over a wide operating range.

Simulation Setup

The simulated system consists of a three-phase AC supply connected to the 270 V DC bus through the AFE rectifier. The supply is modelled at 115 V rms (line-to-line), 400 Hz, with the DC bus reference fixed at 270 V, a converter switching frequency of 10 kHz, and a nominal load resistance of 40 Ω. A Permanent Magnet Synchronous Generator (PMSG) provides the primary source, feeding the AFE through a controlled rectifier stage, while PWM voltages v_{a1}, v_{b1}, and $v_{c1}$are applied at the rectifier input terminals and the DC-link voltage is filtered before entering the control block, as sketched in Figure 3 and implemented in the CRU switching model of Figure 4. Simulations are performed under steady-state, dynamic, and transient conditions, and the key electrical and control parameters are summarized in Table 1.

Steady-State Operation (Nominal load)

Under rated load, the DC bus voltage is tightly regulated around 270 V, and the AC input currents remain nearly sinusoidal while satisfying harmonic distortion limits and operating at approximately unity power factor. In this operating mode, the DC-link reference voltage is set to 270 V and the q-axis current reference $i_q^*$is held at zero, enforcing in-phase operation between the grid voltage and current. Figures 5 and 6 illustrate the resulting steady-state current tracking: Figure 5 shows that the instantaneous d-axis current $i_d$closely follows its reference i_d^*, ensuring accurate DC-link voltage control, whereas Figure 6 confirms that the q-axis current $i_q$tracks $i_q^* = 0$, thereby maintaining unity power factor at the AC input.

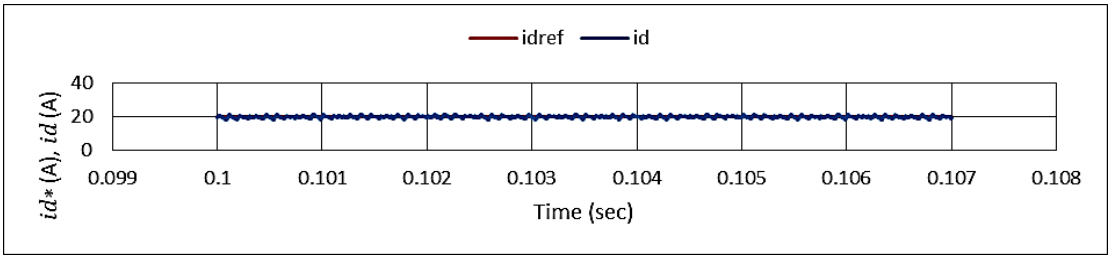

Figure 5. Comparison of reference and instantaneous d-Axis current components ($i_d{}^*$ and i_d)

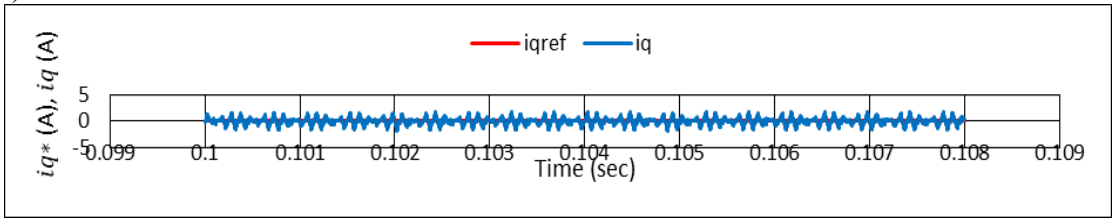

Fig. 6. Comparison of reference and instantaneous q-axis current components ($i_q{}^*$ and i_q)

INTERNATIONAL JOURNAL OF SCIENCE TECHNOLOGY EDUCATION ENTERPRENEURSHIP AND MANAGEMENT
(IJ-STEEM)
ISSN: 3093-0898 Journal homepage: https://atbuijsteem.com.ng/journal

Figure 7 shows the steady-state DC-link voltage response, where the measured voltage rapidly converges to the 270 V reference within approximately 0.1 s, confirming stable and well-damped voltage regulation. The corresponding three-phase line currents in Figure 8 exhibit symmetrical, nearly sinusoidal waveforms with low ripple content, indicating that the total harmonic distortion remains within acceptable limits for automotive power electronics.

Figure 9 further illustrates that the supply phase voltage v_a and current i_a are closely in phase, thereby validating that the system operates at or near unity power factor under nominal conditions. These results collectively demonstrate the effectiveness of the dq-frame control strategy in achieving robust steady-state performance of the 270 V DC bus in EV applications.

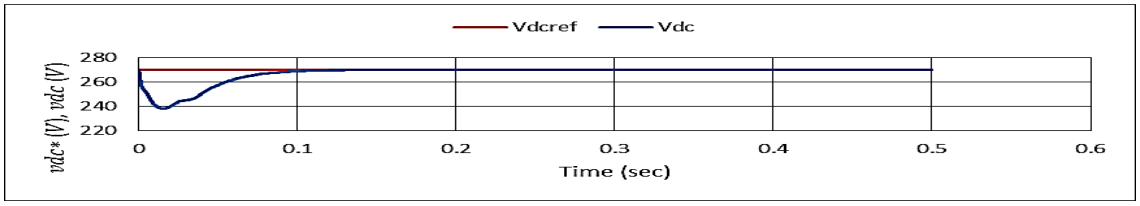

Figure 7. Steady-state waveforms of reference and measured DC-Link Voltage (v_{dc}* and v_{dc})

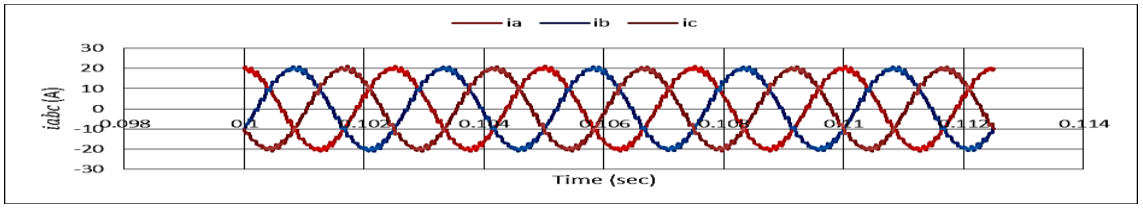

Figure 8. Steady-state waveform of the line currents (i_{abc})

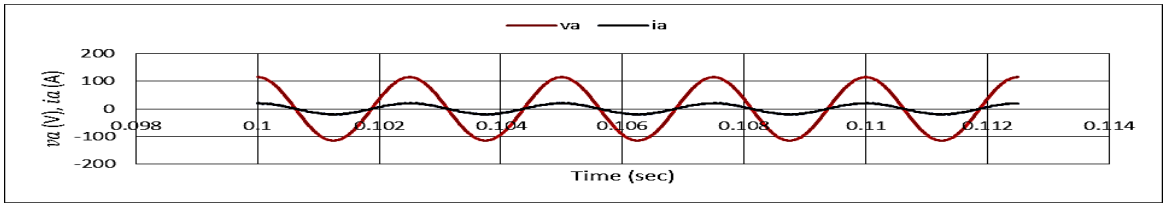

Figure 9. Steady-state waveform of input voltage and current in phase (v_a and i_a)

Step Change in Load

A step change in traction motor demand from 6.25 A to 12.5 A is applied at $t = 0.2$ s. Following this disturbance, the DC bus voltage experiences a transient sag of approximately 10–15 V but rapidly recovers to the 270 V reference within about 0.1 s, as shown in Figure 10, demonstrating the strong dynamic performance of the outer voltage control loop.

Figure 11 shows that the AC source currents increase proportionally with the load while remaining balanced and nearly sinusoidal, confirming correct operation of the AFE under dynamic conditions. As depicted in Figure 12, the supply voltage and current remain

INTERNATIONAL JOURNAL OF SCIENCE TECHNOLOGY EDUCATION ENTERPRENEURSHIP AND MANAGEMENT (IJ-STEEM)
ISSN: 3093-0898 Journal homepage: https://atbuijsteem.com.ng/journal

effectively in phase throughout the transient, preserving unity power factor and validating the effectiveness of the proposed control strategy.

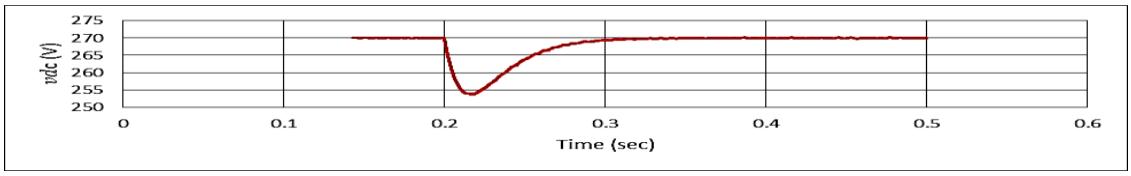

Figure 10. Response of the DC-link voltage (v_{dc}) to a step increase in load current

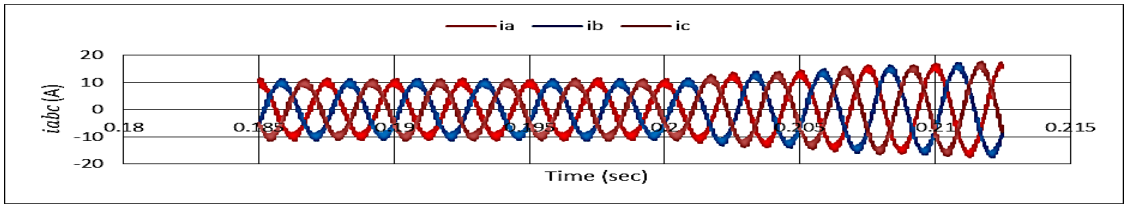

Figure 11. Response of the line currents (i_{abc}) to a step increase of load current

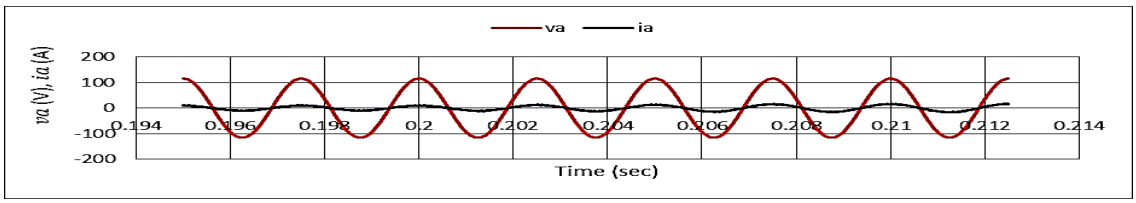

Figure 12. Response of input voltage and current (v_a and i_a) to a step increase of load current

Step Change in DC-Link Voltage

A step change test is performed by increasing the reference DC-link voltage from 270 V to 300 V at $t = 0.2$ s. As shown in Figure 13, the measured DC-link voltage tracks the new reference within roughly 40 ms, highlighting the fast dynamics and robustness of the designed outer voltage controller.

Figures 14 and 15 depict the corresponding current and voltage responses. The higher DC-link reference causes an increase in the d-axis current $i_d$to charge the DC-link capacitor, while the q-axis current $i_q$remains close to zero, so that the line current magnitude rises but the phase alignment between supply voltage and current is preserved, thereby maintaining unity power factor during the transient.

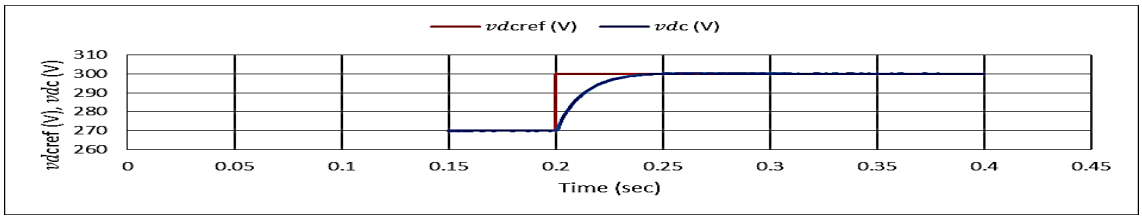

Figure 13. Response of DC-link voltage controller to a 30 V step change in DC-link voltage

INTERNATIONAL JOURNAL OF SCIENCE TECHNOLOGY EDUCATION ENTERPRENEURSHIP AND MANAGEMENT (IJ-STEEM)
ISSN: 3093-0898 Journal homepage: https://atbuijsteem.com.ng/journal

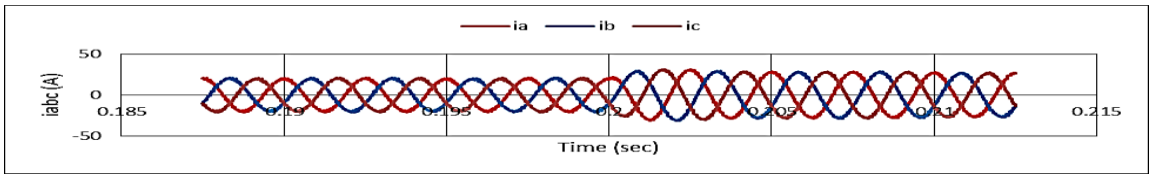

Figure 14. Response of line currents to a 30V step-change in DC-link voltage

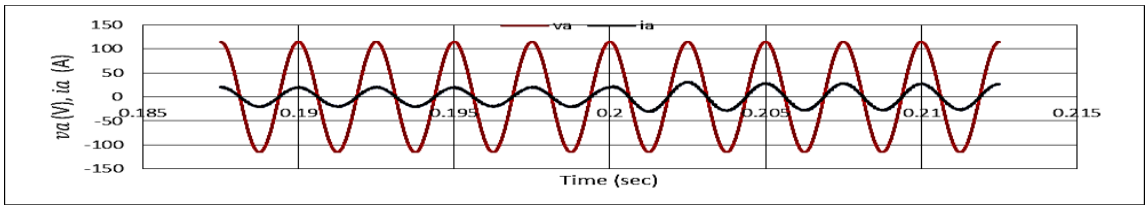

Figure 15. Response of input voltage and current (v_a and i_a) to a 30V step change in DC-link voltage

The simulation results show that the AFE rectifier and its associated control structure are able to maintain tight DC bus regulation over a range of operating conditions, including steady-state, load steps, and DC-link voltage changes. Both transient and steady-state responses exhibit fast recovery following disturbances and high-quality AC-side currents with low harmonic content, confirming the suitability of the proposed 270 V DC system for electric vehicle drive applications and motivating further studies on multi-source and renewable-integrated configurations to assess scalability.

Conclusion

This paper has presented the modelling and simulation of a 270 V DC power system for electric vehicle drive applications, with particular emphasis on the AFE rectifier and its control implementation in the synchronous dq-reference frame. The AFE has been shown to regulate the DC bus voltage effectively while maintaining nearly sinusoidal input currents and high power factor, thereby validating its applicability in modern EV drive architectures that require both power quality and efficiency.The simulation results across different loading scenarios confirm that the proposed system can deliver reliable power to both traction and auxiliary subsystems, even under dynamic operating conditions, and demonstrate that:

i) The AFE rectifier provides robust DC-link voltage regulation.
ii) The dq-based control strategy decouples active and reactive power components, enabling independent control of DC bus voltage and grid-side reactive power; and
iii) The system preserves stability and performance across a wide range of load profiles, underscoring its adaptability for EV applications.

Future work will extend the present single-source framework to multi-source configurations combining grid charging and onboard generation, investigate advanced control approaches such as model predictive and adaptive control to enhance dynamic performance and fault tolerance, and pursue hardware-in-the-loop and experimental validation to translate the simulation findings into practical EV powertrain implementations.

INTERNATIONAL JOURNAL OF SCIENCE TECHNOLOGY EDUCATION ENTERPRENEURSHIP AND MANAGEMENT
(IJ-STEEM)
ISSN: 3093-0898 Journal homepage: https://atbuijsteem.com.ng/journal

References

[1] N. M. Manousakis, P. S. Karagiannopoulos, G. J. Tsekouras and F. D. Kanellos, "Integration of renewable energy and electric vehicles in power systems: a review," Processes, vol. 11, no. 5, p. 1544, 2023.
[2] D. O. Neacșu, Automotive Power Systems, CRC Press, 2020.
[3] Y. Amry, E. Elbouchikhi, F. Le Gall, M. Ghogho and S. El Hani, "Electric vehicle traction drives and charging station power electronics: Current status and challenges," Energies, vol. 15, no. 16, p. 6037, 2022.
[4] R. Pradhan, N. Keshmiri and A. Emadi, "On-board chargers for high-voltage electric vehicle powertrains: Future trends and challenges," IEEE Open Journal of Power Electronics, vol. 4, pp. 189-207, 2023.
[5] H. M. Hussein, A. M. Ibrahim, R. A. Taha, S. S. H. Rafin, M. S. Abdelrahman, I. Kharchouf and O. A. Mohammed, "State-of-the-Art Electric Vehicle Modeling: Architectures, Control, and Regulations," Electronics, vol. 13, no. 17, p. 3578, 2024.
[6] H. Hussaini, T. Yang, G. Bai, M. Urrutia-Ortiz and S. Bozhko, "Artificial Intelligence-Based Hierarchical Control Design for Current Sharing and Voltage Restoration in DC Microgrid of the More Electric Aircraft," IEEE Transactions on Transportation Electrification, vol. 10, no. 1, pp. 566-582, March 2024.
[7] R. R. Sarangi, P. K. Ray, A. Mohanty, S. Khadem and S. Patra, "Enhancing DC microgrid security: A comprehensive review of protection challenges and solutions," International Journal of Electrical Power & Energy Systems, vol. 168, no. 110687, 2025.
[8] R. T. Hock, Y. R. de Novaes and A. L. Batschauer, "A voltage regulator for power quality improvement in low-voltage distribution grids," IEEE Transactions on Power Electronics, vol. 33, no. 3, pp. 2050-2060, 2017.
[9] D. E. Quevedo, R. P. Aguilera, M. A. Perez, P. Cortes and R. Lizana, "Model predictive control of an AFE rectifier with dynamic references," IEEE Transactions on Power Electronics, vol. 27, no. 7, pp. 3128-3136, 2011.
[10] J. M. Cano, J. Jatskevich, J. G. Norniella, A. Davoudi, X. Wang, J. A. Martinez and D. C. Aliprantis, "Dynamic average-value modeling of direct power-controlled active front-end rectifiers," IEEE Transactions on Power Delivery, vol. 29, no. 6, pp. 2458-2466, 2014.
[11] S. Kallio, M. Andriollo, A. Tortella and J. Karttunen, "Decoupled dq model of double-star interior-permanent-magnet synchronous machines," IEEE Transactions on Industrial Electronics, vol. 60, no. 6, pp. 2486-2494, 2012.
[12] A. Guha and G. Narayanan, "Average modelling of a voltage source inverter with dead-time in a synchronous reference frame," in 2013 IEEE Innovative Smart Grid Technologies-Asia (ISGT Asia), 2013.
[13] Q. C. Zhong and T. Hornik, "Cascaded current–voltage control to improve the power quality for a grid-connected inverter with a local load," IEEE Transactions on Industrial Electronics, vol. 60, no. 4, pp. 1344-1355, 2012.
[14] M. Popat, B. Wu and N. R. Zargari, "DC link current control of cascaded current source converter based offshore wind farms," in 2011 IEEE International Electric Machines & Drives Conference (IEMDC), 2011.

INTERNATIONAL JOURNAL OF SCIENCE TECHNOLOGY EDUCATION ENTERPRENEURSHIP AND MANAGEMENT
(IJ-STEEM)
ISSN: 3093-0898 Journal homepage: https://atbuijsteem.com.ng/journal

[15] X. Wang, X. Ruan, S. Liu and C. K. Tse, "Full feedforward of grid voltage for grid-connected inverter with LCL filter to suppress current distortion due to grid voltage harmonics," IEEE Transactions on Power Electronics, vol. 25, no. 12, pp. 3119-3127, 2010.

[16] W. H. Chen, J. Yang, L. Guo and S. Li, "Disturbance-observer-based control and related methods—An overview," IEEE Transactions on industrial electronics, vol. 63, no. 2, pp. 1083-1095, 2015.

[17] S. Tarbouriech and M. Turner, "Anti-windup design: an overview of some recent advances and open problems," IET control theory & applications, vol. 3, no. 1, pp. 1-19, 2009.

[18] X. He and H. Geng, "PLL synchronization stability of grid-connected multiconverter systems," IEEE Transactions on Industry Applications, vol. 58, no. 1, pp. 830-842, 2021.

[19] L. F. A. Pereira and A. S. Bazanella, "Tuning rules for proportional resonant controllers," IEEE Transactions on Control Systems Technology, vol. 23, no. 5, pp. 2010-2017, 2015.

[20] V. Mihaly, M. Şuşcă, D. Morar, M. Stănese and P. Dobra, "μ-synthesis for fractional-order robust controllers," Mathematics, vol. 9, no. 8, p. 911, 2021.

[21] C. E. Garcia, D. M. Prett and M. Morari, "Model predictive control: Theory and practice—A survey," Automatica, vol. 25, no. 3, pp. 335-348, 1989.

[22] S. Zhou, J. Liu and Y. Zhang, "A decoupling method based on reference current feedforward for DQ-frame PI current control of grid-connected voltage source converters," in 2015 IEEE 2nd International Future Energy Electronics Conference (IFEEC), 2015.

[23] K. V. Kumar, P. A. Michael, J. P. John and S. S. Kumar, "Simulation and comparison of SPWM and SVPWM control for three phase inverter," ARPN journal of engineering and applied sciences, vol. 5, no. 7, pp. 61-74, 2010.

[24] G. M. Silva and L. C. Kretly, "Electromagnetic shielding of a Bluetooth antenna for electric vehicles applying metamaterial structures," in 2021 IEEE International Conference on Microwaves, Antennas, Communications and Electronic Systems (COMCAS), 2021.

[25] A. Fazeli, M. Zeinali and A. Khajepour, "Application of adaptive sliding mode control for regenerative braking torque control," IEEE/ASME Transactions On Mechatronics, vol. 17, no. 4, pp. 745-755, 2011.

[26] S. Bozhko, S. S. Yeoh, F. Gao and C. Hill, "Aircraft starter-generator system based on permanent-magnet machine fed by active front-end rectifier," in IECON 2014 - 40th Annual Conference of the IEEE Industrial Electronics Society (pp. 2958-2964). IEEE, Dallas, TX, USA, 29 Oct.-1 Nov. 2014.

[27] V. Dargahi, M. Abarzadeh, K. A. Corzine, J. H. Enslin, A. K. Sadigh, J. Rodriguez and A. Maqsood, "Fundamental circuit topology of duo-active-neutral-point-clamped, duo-neutral-point-clamped, and duo-neutral-point-piloted multilevel converters," IEEE Journal of Emerging and Selected Topics in Power Electronics,, vol. 7, no. 2, pp. 1224-1242, 2018.

INTERNATIONAL JOURNAL OF SCIENCE TECHNOLOGY EDUCATION ENTERPRENEURSHIP AND MANAGEMENT
(IJ-STEEM)
ISSN: 3093-0898 Journal homepage: https://atbuijsteem.com.ng/journal

[28] Y. Ye, M. Kazerani and V. H. Quintana, " Modeling, control and implementation of three-phase PWM converters," IEEE Transactions on Power electronics, vol. 18, no. 3, pp. 857-864, 2003.

[29] P. P. Pandit, "Modeling and analysis of active front-end induction motor drive for reactive power compensation.," Maters Thesis, University of Tennessee, Knoxville, 2005.

[30] C. C. Azevedo, R. L. A. Ribeiro, C. B. Jacobina and R. M. Sousa, "DC-link regulator for shunt power active filter using feed-forward control strategy," in XI Brazilian Power Electronics Conference (pp. 877-883). IEEE, Praiamar, Brazil, 2011, September.

[31] M. Liserre, A. Dell'Aquila and F. Blaabjerg, "Design and control of a three-phase active rectifier under non-ideal operating conditions," in Conference Record of the 2002 IEEE Industry Applications Conference. 37th IAS Annual Meeting (Cat. No.02CH37344), Pittsburgh, PA, USA, USA, October, 2002.

[32] M. N. Stefanos, "Inverters (DC–AC Converters)," in Power Electronics and Motor Drive Systems, Academic Press, 2017, pp. 271-500.

[33] T. Wu, S. V. Bozhko, G. M. Asher and D. W. Thomas, "Fast functional modelling of the aircraft power system including line fault scenarios.," in 5th IET International Conference on Power Electronics, Machines and Drives (PEMD 2010), Brighton, UK, UK, 2010.

[34] E. M. Suhara and M. Nandakumar, "Voltage oriented control of three phase PWM rectifier with Bus Clamped Space Vector PWM," in 2015 International Conference on Power, Instrumentation, Control and Computing (PICC) (pp. 1-5). IEEE., Thrissur, India, December, 2015.